HIGH SCHOOL EDITION
Journal of Student Research
Volume 12 Issue 4 (2023)

K-band Absolute Magnitude Relations of Red Clump Stars Separated by Age

Tiffany Zhang[1] and Nicole Spinelli[#]

[1]Great Neck South High School
[#]Advisor

ABSTRACT

Red clump (RC) stars form a distinguishable clump on the color-magnitude diagram, making it a good distance indicator. Currently, the two main absolute magnitude estimation methods in the I-band (700–900 nm) conflict: one assumes a constant RC magnitude as supported by empirical data and one relates magnitude with other physical characteristics as supported by theoretical models. Studies attribute these discrepancies to population effects, such as dust, and recommend the K-band (2000–2400 nm) to minimize them. Past studies analyzed relations between the K-band magnitude, color, metallicity, and age, including those stratified by age at 2 Gyr. This study aims to investigate these different relations to clarify trends from past studies, discover new trends, and compare them to similar relations in the I-band. After analyzing cluster RC data from *Gaia* DR3, 2MASS, and *Gaia*-ESO DR5, K-band magnitude exhibits insignificant correlation in all relations ($p>0.05$) but has the greatest dependence and the least root mean square error (RMS) with metallicity in the old RC. Significant correlation was found between I-band magnitude and metallicity for all RC and young RC ($p<0.05$), especially the latter ($R^2 = 0.804$). This consistency with theoretical trends suggests weaker I-band population effects than previously believed. Overall, these three relations yield more accurate predictions than the mean magnitude. Thus, studies cannot solely rely on the mean K-band or I-band magnitude to estimate distance, and magnitude relations stratified by age can potentially lead to more accurate RC distance estimations and a more accurately calibrated distance ladder.

Introduction

Red clump (RC) stars are core helium-burning, low-mass horizontal branch stars and clump based on consistent magnitude on the color–magnitude diagram (CMD) (Fig. 1). The CMD distinguishes stars at different stages in its evolution by plotting absolute magnitude of a passband (intrinsic brightness of a specific wavelength range) against color (calculated by the difference of magnitudes of two different passbands, or the wavelength ranges where light can pass through a filter and be measured). Note that increasing magnitude corresponds to decreasing brightness (Eq. 1).

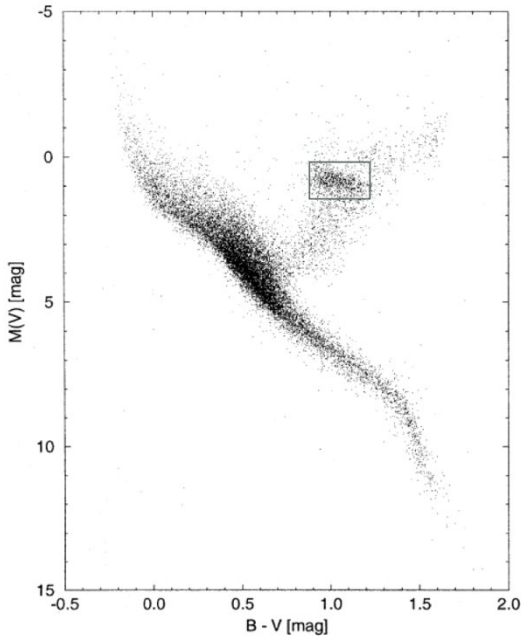

Figure 1. Color–magnitude diagram from Hipparcos data. The V-band (500–700 nm) magnitude is plotted against B-V color, or the color calculated from the difference of the B-band (400–500 nm) and V-band magnitude. The axis is inverted to represent upwards as increasing brightness, or decreasing magnitude. The box added by the author demarcates the red clump (Perryman, 1997).

Equation 1: Definition of magnitude

$$m = -2.5 \log(F/F_0)$$

where m is the magnitude, flux F is the measured energy emitted per second per unit area, and the zero-point flux F_0 is the flux of a star, usually Vega, set as the baseline assigned by the observer to calibrate and maintain consistency among the measurements (Reid, 1999). Since magnitude changes with distance, the absolute magnitude is defined as the observed magnitude if the object were at a fixed distance of 10 pc away from the observer.

The RC's clumping on the CMD is caused by its consistent mass from undergoing a previous stage of degeneracy. In this stage, the core mass stops changing with temperature and pressure after fusing all the core hydrogen into helium, which cannot be fused with the core's low temperatures (Girardi, 2016). Since mass dictates the rate of elements being fused and light emitted, a consistent mass leads to a consistent absolute magnitude. Moreover, RC stars are far more abundant than horizontal branch stars and consist of about one-third of red giant branch stars, making the clump especially prominent on the CMD (Girardi, 2016).

Because of the RC's distinguishable clumping, Canon (1970) became the first study that suggested its use as a distance indicator, or an astronomical object used to estimate absolute magnitude and calculate distance with the distance modulus equation (Eq. 2).

Equation 2: Distance modulus equation

$$m - M = -5 + 5 \log d$$

where m is the apparent magnitude, or the observed magnitude measured with photometry, M is the absolute magnitude, and d is the distance. Distance indicators only cover a limited range of distances as they might not be present

within a certain distance range or become too faint outside a certain distance range. Consequently, new distance indicators are needed to verify distance estimations and calibrate other distance indicators to measure farther unknown distances. This forms a distance ladder, where distance indicators that cover a closer distance range calibrate those that cover a farther distance range (Reid, 1999).

Because of the RC's consistent magnitude, Canon (1970) saw that its absolute magnitude could be estimated by assuming the mean magnitude from an RC sample as constant across the entire RC. This is later supported by Paczyński & Stanek (1998), who found a lack of variation of the passband I-band (700–900 nm) magnitude with color in empirical data from the OGLE and Hipparcos database and became the first significant study evaluating the RC as a distance indicator. Furthermore, Uldalski (1999, 2000) found a lack of variation of the I-band magnitude with relation to metallicity or age. Because of this estimation method's simplicity, it became widely used for distance estimations.

Despite the earliest studies supporting the absolute magnitude estimation method of assuming a constant magnitude in the I-band, later studies found conflicting trends that suggest otherwise. Contrary to empirical data, theoretical models found variation in the I-band that can be attributed to systematic trends with metallicity and age as their fitted lines had a substantial trend (Sarajedini, 1999; Girardi & Salaris, 2001). This suggests a different absolute magnitude estimation method: calibrating a magnitude function of other physical characteristics (e.g. color, metallicity, and age).

The discrepancies between empirical and theoretical data suggests that one of these estimation methods is inaccurate and can lead to inaccurate distance estimations. Pietrzyński et al. (2010) attributes these discrepancies to strong I-band population effects, or differences between actual and observed data caused by external factors altering the light observed, such as dust between the source and the observer, assuming theoretical models reflect the actual trends. By reacting with high energy photons and taking away their energy, dust can lead to extinction and reddening, or decreases in amplitude (intensity) and wavelength (blueness) of light, respectively. Extinction and reddening are quantified by the difference between the apparent and absolute magnitude and the difference between the observed and intrinsic color, respectively. The I-band is susceptible to these effects because of its relatively short wavelengths that provide enough energy for these reactions to occur. Consequently, Pietrzyński et al. (2010) recommends near-infrared passbands with longer wavelengths because their lower frequencies allow them to pass through dust more easily and reduce these reactions because of their small size and low energy, thereby minimizing population effects.

The most popular of the recommended passbands is the near-infrared passband K-band (2000–2400 nm), and past studies investigated different RC relations with the K-band magnitude, color J-K (calculated from the difference of the J-band (1000–1400 nm) and K-band magnitudes), metallicity, and age. Alves (2000), the first study using the K-band for its long wavelength to minimize population effects and analyze the RC as a distance indicator, found a lack of variation in the K-band magnitude with metallicity; later studies showed similar results (e.g. Pietrzynski et al., 2003; Laney et al., 2012). Similarly, Bilir et al. (2013b) and Grocholski & Sarajedini (2002) found negligible variation in K-band magnitude with metallicity. However, upon analyzing the K-band magnitude in relation with metallicity and age stratified by age, Grocholski & Sarajedini (2002) found that the K-band magnitude of RC stars younger than ~2 Gyr exhibits sensitivity (and an increasing trend) with age but not metallicity while those older than ~2 Gyr exhibits sensitivity (and a decreasing trend) with metallicity but not age. However, past studies have not yet analyzed the I-band relations stratified by age. Since color is dependent on metallicity and age in the RC (Nataf et al., 2021), it is possible that the K-band magnitude is dependent on color stratified by age.

Therefore, this study aims to analyze K-band relations stratified by age at 2 Gyr with magnitude, color, metallicity, and age to clarify trends in the RC found by past studies, discover new trends, and compare them to similar relations in the I-band stratified by age.

Methods

Cluster Data Collection

Clusters were selected from Jackson et al. (2021), Bilir et al. (2013a), Grocholski & Sarajedini (2002), and other papers for distance modulus, reddening, and age based on availability of each cluster's data on the databases Two Micron All Sky Survey (2MASS), *Gaia* DR3, and *Gaia*-ESO DR5, totaling to 53 clusters. In the following equations, the reddening of the color B-V, denoted as E(B-V), can be converted to the reddening of the color J-K and extinction of the K-band magnitude, denoted by E(J-K) and A_K, respectively: $A_V = 3.2E(B-V)$, $A_K = 0.689E(J-K)$, and $A_K/A_V = 0.112$ (Gonzalez et al. (2012); Rieke & Lebofsky (1985)).

The data for each cluster is queried from the 2MASS, *Gaia* DR3, and *Gaia*-ESO DR5: stellar coordinates of right ascension and declination and their respective errors, parallax, and the J-band and K_S-band apparent magnitudes were obtained from 2MASS and *Gaia*, which were crossmatched with the crossmatching system in the *Gaia* catalogue and saved as .csv files (Marrese et al. 2019). Note that the K_S-band magnitude was converted to the K-band magnitude with the conversion $M_K = M_{K_S} + 0.044$ (Grocholski & Sarajedini, 2002). The right ascension, declination, effective temperature, surface gravity, and metallicity were obtained from *Gaia*-ESO and saved as .csv files as well.

Since the distance to each of the stars in the same star cluster is normally distributed, the cluster data was filtered based on parallax, an indirect measurement of distance whose reciprocal calculates distance (Fig. 2). Stars with parallax outside ±2 standard deviations of the mean were removed, and clusters with a calculated mean distance inconsistent with the cluster distance obtained from previous studies (i.e. outside ±1 standard deviation of the mean) are removed as well.

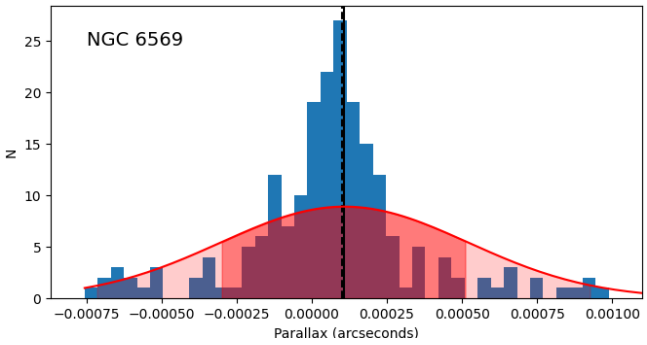

Figure 2. Parallax distribution of NGC 6569. The dotted and solid line represent the actual and mean parallax, respectively. Each red shaded region under the red parallax probability density function represents ±1 standard deviation.

Red Clump Isolation

The RC was isolated by creating CMDs for each cluster, manually identifying the RC's K-band magnitude and color range by its overdensity, and separating the data for analysis (Fig. 3).

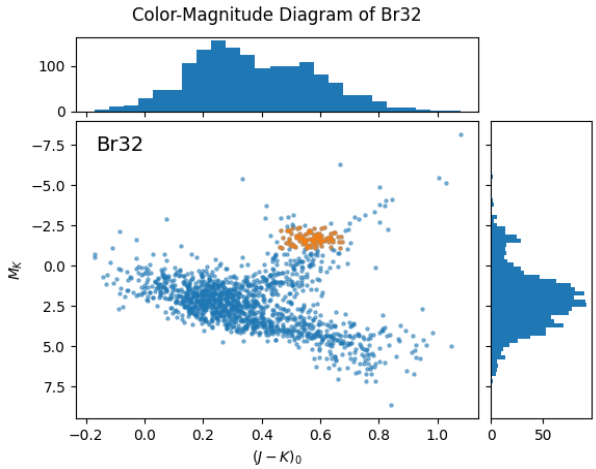

Figure 3. Color-magnitude diagram of Berkeley 32 (Br32). The stars of Br32 are plotted in blue and the RC in orange. The subplots along the y- and x-axis present histograms of the K-band magnitude and color distributions, respectively, and emphasize the overdensities in the K-band magnitude and color ranges.

However, because of the contaminants that reside near the RC on the CMD, including the cooler and less luminous red giant branch stars and less luminous secondary red clump (Fig. 4), the RC cannot be isolated by solely identifying the overdensity.

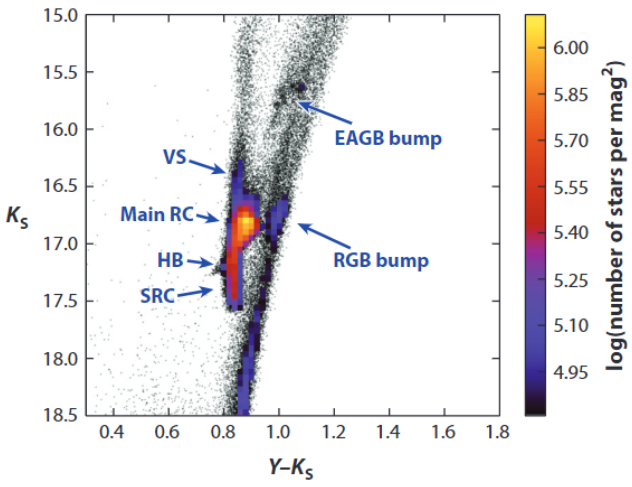

Figure 4. CMD from a Large Magellanic Cloud Simulation. Various substructures from different star stages reside near the RC. Note that the substructure abbreviations VS stand for vertical structure, HB for horizontal branch, SRC for secondary red clump, RGB for red giant branch, and EAGB for early asymptotic giant branch (Girardi, 2016).

The effective temperature versus surface gravity plots (T_{eff} vs. log *g* plots) can filter out contaminants because asteroseismic parameters are considered more reliable than spectroscopic parameters as noted by Girardi (2016). Hence, to filter out contaminants of the manually isolated RCs, the cuts of Equation 3 from Bovy et al. (2014) as depicted in purple in Figure 5 were used.

Equation 3: Effective temperature and surface gravity cuts (Bovy et al., 2014)

$$1.8 \leq log\ g \leq 0.0018 \text{ dex K}^{-1} \left(\mathrm{T_{eff}} - \mathrm{T_{eff}^{ref}}([\mathrm{Fe/H}])\right) + 2.5$$

where $T_{\mathrm{eff}}^{\mathrm{ref}}([\mathrm{Fe/H}])$ is defined as $-382.5 \text{ K dex}^{-1}\ [\mathrm{Fe/H}] + 4607\mathrm{K}$.

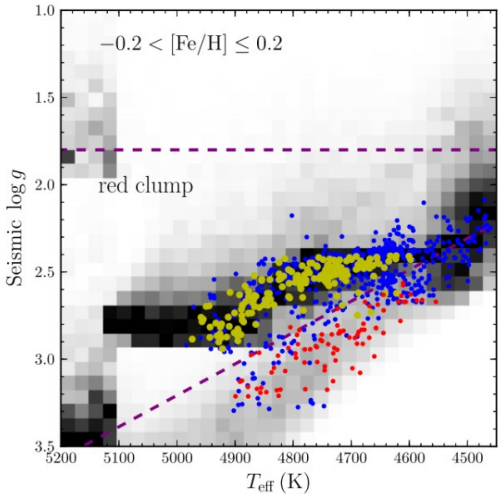

Figure 5. Effective temperature vs surface gravity plot. The purple cuts from Equation 3 distinguish the RC in yellow from the contaminant RGB in red. The black and white background represents the isochrone, or stellar evolution path, that the RC and RGB are predicted to reside on (Bovy et al., 2014)

Data Analysis

After calculating its mean magnitude, color, and metallicity, each cluster's RC represents one datapoint, as shown in Supplementary Table 1, to eliminate intrinsic variation within the cluster and analyze the different K-band magnitude relations with color, metallicity, and age stratified by age at 2 Gyr. The R^2-coefficients and p-values were evaluated through Ordinary Least Squares (OLS) regression to determine the dependence and its significance, respectively, and the root mean square error (RMS) to determine the error of the regression. To compare the K-band magnitude relations with the I-band, RC data from Pietrzyński et al. (2010) and other studies were collected as shown in Supplementary Table 2 and the same magnitude relations of color, metallicity, and age stratified by age in the I-band were analyzed.

Additionally, Girardi (2016) suggests a multiband approach to minimize error by averaging the distance predictions from different passbands, thereby averaging offsets. Hence, the distance predictions from the two estimation methods (i.e. assuming a constant magnitude and calculating the magnitude with a relation) in the K-band, I-band, and averaging those in the K- and I-band were analyzed, and their RMS were compared.

Aside from the magnitude relations, the relation between metallicity and age was examined to determine whether the RC exhibits a positive trend consistent with stellar evolution models, where elements fuse to form heavier ones, or a downward trend consistent with star formation models, where stars that formed later in metal-rich interstellar medium have higher metallicities than stars that formed earlier in metal-poor interstellar medium.

Testing

The accuracy of the relation was assessed by plotting estimated magnitudes calculated from the relations against actual magnitudes from the original queried cluster data (Bilir et al., 2013a). The identity line (y=x) and the identity lines shifted vertically by ±1 RMS were plotted to visualize skewness and accuracy (Fig. 6).

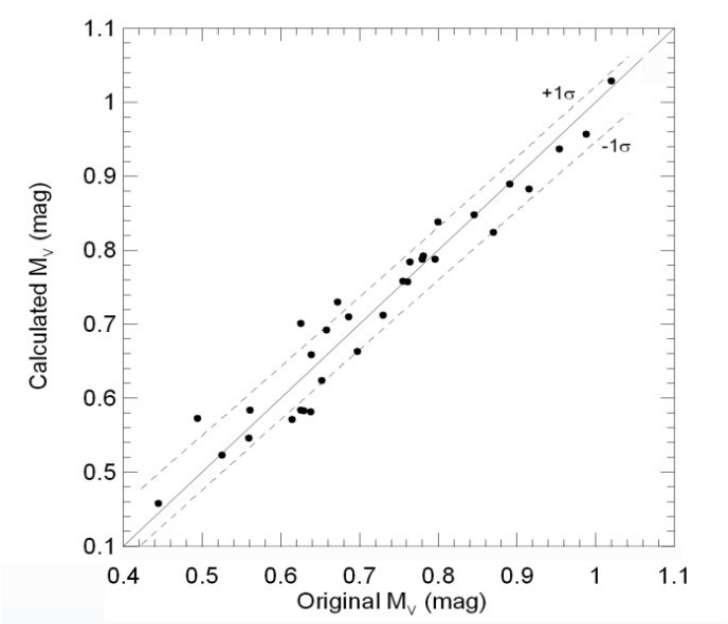

Figure 6. Estimated vs. actual V-band (500–700 nm) magnitude plots. The estimated V-band magnitudes from the relations and the actual V-band magnitudes from the original data as well as the identity line and the lines shifted vertically by ±1 RMS from the identity line were plotted (Bilir et al., 2013a).

Results

The K-band metallicity-luminosity relation of old red clump stars exhibits the greatest dependence and least error, but the K-band relations demonstrate no significant correlation.

After calculating the properties of each cluster's RC, the data was stratified by age at 2 Gyr, examined with OLS analysis, and plotted with its regression as shown in Figure 7. Note that the y-axis is inverted, so up represents decreasing magnitude and increasing luminosity.

The color-metallicity relation exhibits an inverse relation for all the RC (R^2=0.101), the old RC (R^2=0.058), and the young RC (R^2=0.067) (Fig. 7a); the metallicity-luminosity relation exhibits an inverse relation for all the RC (R^2=0.116) and the old RC (R^2=0.244) but a direct relation for the young RC (R^2=0.004) (Fig. 7b); and the age-luminosity relation exhibits an inverse relation for the young RC (R^2=0.077), direct relation for the old RC (R^2=0.139), and a subtle direct relation for all the RC (R^2=0.001) (Fig. 7c). However, these relations are insignificant ($p>0.05$), and data is missing from much of the metallicity-luminosity fit line, especially in the range $-1.0 \leq [Fe/H] \leq -0.4$.

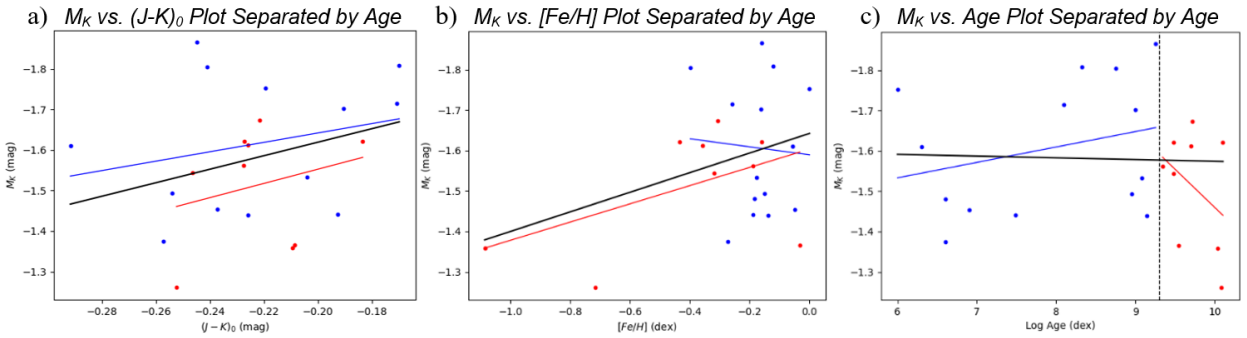

Figure 7. K-band magnitude relations with color, metallicity, and age stratified by age (n=24). The young and old red clump are stratified at 2 Gyr and represented in blue and red, respectively, while the relation of all the red clump is represented in black. The dotted line in Fig. 7c divides the plot at 2 Gyr. Note that the y-axis is inverted, so up represents decreasing magnitude and increasing luminosity.

The R^2-coefficients and RMS were evaluated in the regression of analysis of these K-band magnitude relations to evaluate the extent of the dependence and the accuracy of the model, respectively. Table 1 presents the R^2-coefficients and RMS, and those of the color-luminosity relation, greatest R^2-coefficient, and lowest RMS are in bold. While the K-band magnitude exhibited little dependence on color in all categories, the metallicity-luminosity relation of the old RC exhibited the greatest dependence and least error out of all the K-band magnitude relations and can potentially yield accurate distance predictions.

Table 1. R^2-coefficients and root mean square errors of all RC regressions. After conducting OLS analysis on the K-band RC data, the R^2-coefficients and RMS are evaluated and those of the color-luminosity relations, the highest R^2-coefficient, and the lowest RMS are in bold.

	R^2-coefficient			**RMS**		
	Color	**[Fe/H]**	**Age**	**Color**	**[Fe/H]**	**Age**
All M_K	**0.101**	0.116	0.001	**0.158**	0.153	0.163
Young M_K	**0.067**	0.004	0.077	**0.156**	0.159	0.153
Old M_K	**0.058**	**0.244**	0.139	**0.134**	**0.120**	0.128

Significant correlation was found in the I-band metallicity-luminosity relation of all the red clump and the young red clump, especially the latter.

With cluster red clump data from Pietrzyński et al. (2010) and other studies, similar magnitude relations in the I-band were analyzed and their R^2-coefficients and RMS evaluated.

The metallicity-luminosity relation of all and the young RC exhibited significant correlation ($p<0.05$), especially in the young RC with an R^2-coefficient of 0.804 and RMS of 0.182 compared to the R^2-coefficient of 0.681 and RMS of 0.179 in all the RC (Fig. 8). In all categories of the RC, the I-band magnitude and metallicity exhibited a direct relation. The other I-band magnitude relations are insignificant ($p>0.05$), and the results of their regression analysis are presented in Supplementary Table 3.

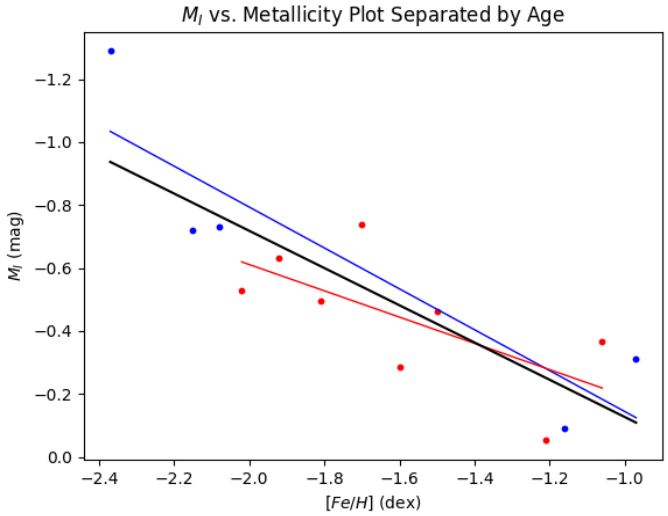

Figure 8. I-band metallicity-luminosity relation stratified by age (n=13). I-band cluster data from Pietrzyński et al. (2010) and other studies were stratified by age at 2 Gyr and analyzed to compare the K-band magnitude relations with those of the I-band. The young RC and its regression are plotted in blue, old RC and its regression in red, and the regression of all the RC in black.

The metallicity-luminosity relations of the old red clump in the K-band and of the young red clump and all the red clump in the I-band yield more accurate predictions than the mean magnitude.

Estimated magnitude vs. actual magnitude plots with the identity line (y=x) and the identity lines shifted vertically by ±1 RMS were plotted to test the potential of the K-band metallicity-luminosity relation of the old RC and the I-band metallicity-luminosity relation of the young RC and all the RC. Below are the relations from the regression analysis to estimate absolute magnitude.

Equation 4: K-band metallicity-luminosity relation of the old red clump

$$M_{K,\text{old}} = (-0.2254 \pm 0.150)[\text{Fe/H}] + (-1.6033 \pm 0.075)$$

Equation 5: I-band metallicity-luminosity relation of all the red clump

$$M_{I,\text{all}} = (0.5916 \pm 0.122)[\text{Fe/H}] + (0.4649 \pm 0.209)$$

Equation 6: I-band metallicity-luminosity relation of the young red clump

$$M_{I,\text{young}} = (0.6496 \pm 0.186)[\text{Fe/H}] + (0.5056 \pm 0.340)$$

Additionally, a horizontal line representing the mean magnitude estimation was plotted to compare the absolute magnitude estimation methods on the collected data. Almost all predictions from the relations reside within one RMS of the identity line and yield more accurate predictions than the mean magnitude (Fig. 9).

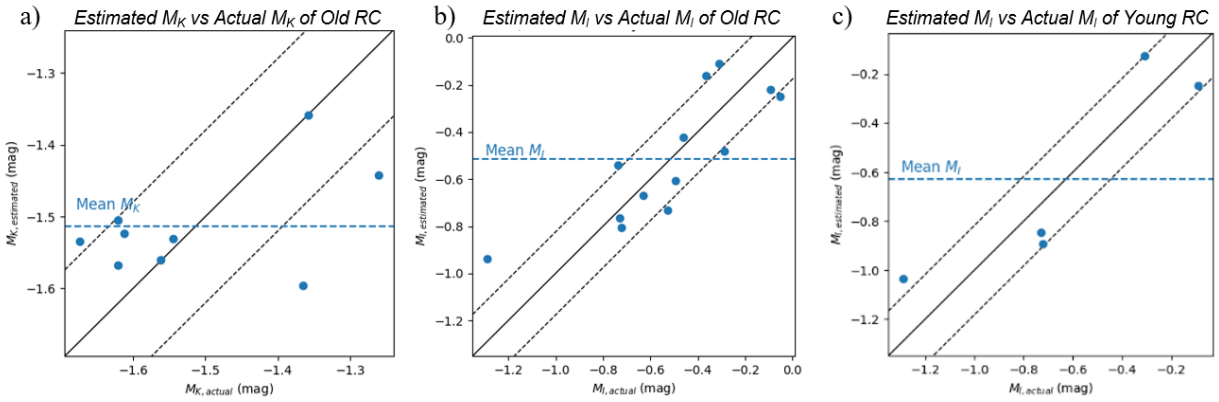

Figure 9. Estimated magnitude vs. actual magnitude of metallicity-luminosity relations of the old RC in the K-band and of all the RC and the young RC in the I-band. The estimated magnitudes are determined from the regressions (Equations 4, 5, & 6), and the actual magnitudes from the original queried data. The identity line, the identity lines shifted vertically by ±1 RMS, and a horizontal line of the mean magnitude were plotted to compare the two estimation methods and their accuracy.

The multiband approach with the K-band and I-band mean magnitudes yields more accurate predictions than the multiband approach with K-band and I-band relations.

As suggested by Girardi (2016), a multiband approach by averaging the distance predictions can average offsets and minimize error. With K-band and I-band red clump cluster data from Percival & Salaris (2003) presented in Supplementary Table 4, the relations are analyzed and compared with testing data different from the original regression data.

Table 2 presents the RMS of the distance modulus predictions for both estimation methods in the I-band, the K-band, and the multiband approach. Since the K-band metallicity-luminosity relation of the old RC had the greatest potential among the K-band relations, only the old K- and I-band RC data was analyzed to evaluate the target K-band relation and maintain consistency in the RMS analysis among the K-band and I-band relations. Consequently, the I-band metallicity-luminosity relation of all the RC was analyzed despite the I-band metallicity-luminosity relation of the young RC having greater potential.

While the distance predictions from the K-band relation had less error than those from the mean K-band magnitude, those from the I-band relation and from the multiband approach of the relations had more error than those from the I-band mean magnitude and from the multiband method of the mean magnitudes, respectively (Table 2).

Table 2. Root mean square errors of the distance modulus predictions in the multiband approach. With the testing cluster data from Percival & Salaris (2003), both distance estimation methods in the K-band and I-band and the multiband method were analyzed and compared.

RMS		
	Relation	**Mean Magnitude**
K-band	0.137	0.174
I-band	0.493	0.369
Average	0.222	0.204

Metallicity and age exhibit an inverse relation in red clump stars.

Besides the magnitude relations, the relation between metallicity and age was analyzed to determine whether the RC exhibits a positive or negative trend. Figure 9 displays the negative trend between metallicity and age in the K-band (R^2=0.248). This suggests that RC trends must be consistent with those of star formation models instead of stellar evolution models.

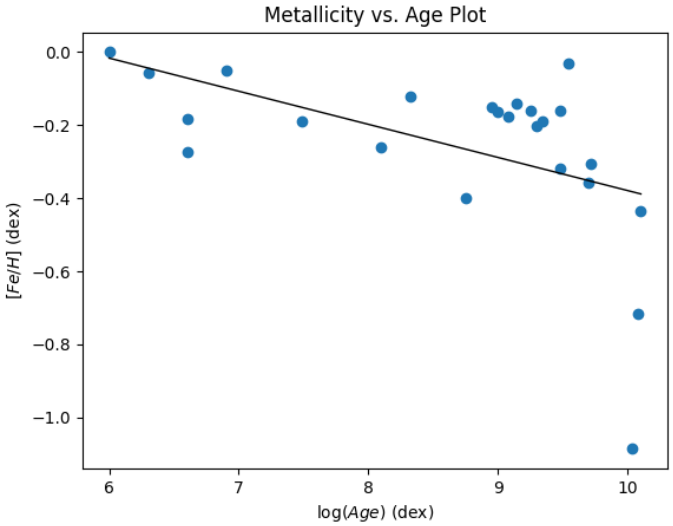

Figure 10. Metallicity vs. age plot of the red clump. The K-band red clump data was plotted, and a line was fitted to illustrate the direction of the trend.

Discussion

The objective of this study was to analyze various K-band relations to clarify trends in the RC found by past studies, discover new ones, and compare them to similar relations in the I-band.

The trends of the K-band magnitude with color, metallicity, and age are mostly consistent with past studies. The color-luminosity relation exhibited insignificant correlation and an inverse relation, consistent with Bilir et al. (2013b) even though the past study found similar results between the K_S-band magnitude and the color J-H. The metallicity-luminosity relation exhibited insignificant correlation in all categories, an inverse relation in all and the old RC, a direct relation in the young RC, and greater dependence in the old RC than the young RC, while the age-luminosity relation exhibited insignificant correlation and a direct relation in all the RC and the old RC, consistent with the empirical data from Grocholski & Sarajedini (2002) and the theoretical trends from Girardi (2016). However, the young age-luminosity relation exhibits a direct relation, and the K-band magnitude is less dependent in the young RC than the old RC, inconsistent with Grocholski & Sarajedini (2002), who found an inverse relation and greater dependence in the young RC. This is likely because this study's age range extends below the lower limit of that in Grocholski & Sarajedini (2002), causing the scatter of the young age-luminosity data to resemble a polynomial fit consistent with theoretical models (Girardi, 2016). The overall consistency of this study's empirical data with theoretical models and other empirical studies suggests that the population effects were minimized and likely validates the data in the K-band.

The K-band metallicity-luminosity relation of the old RC and the I-band metallicity-luminosity relation of all the RC and the young RC demonstrate the greatest potential for distance estimations. Along with its consistency with previous studies, the K-band magnitude has the greatest dependence and the least RMS on metallicity in the old RC. While data is missing from much of the fit line and the regression coefficient is insignificant, the metallicity range of the I-band RC data extends below the lower bound of the metallicity range of the K-band RC data, suggesting that

this K-band trend may become more apparent with more data. Furthermore, when tested against new data from Percival & Salaris (2003), the K-band relation produced the lowest RMS among the other distance estimation methods, including the K-band mean magnitude. Along with the estimated vs. actual magnitude plots, the K-band relation—and the I-band relations—more accurately predicted absolute magnitudes than the more commonly used method of assuming a constant magnitude, validating the use of the K-band metallicity-luminosity relation of the old RC for distance estimations over the mean magnitude method. Similarly, in addition to the significant correlation, high R^2-coefficients, and low RMS of I-band metallicity-luminosity relations of all the RC and the young RC, the estimated vs. actual magnitude plots illustrated the more accurate distance predictions of the I-band relation compared to the mean I-band magnitude. However, the I-band relation produced a greater RMS than the I-band mean magnitude when tested against new data from Percival & Salaris (2003). This was likely due to the lack of the I-band relation's fit with the old RC as it was calibrated with all the RC. Overall, the K-band and I-band relations stratified by age demonstrated greater accuracy in distance predictions than the K-band and I-band mean magnitudes.

While discrepancies in empirical and theoretical data in the I-band leave debates on the best absolute magnitude estimation method unresolved, this study found significant correlation in the I-band metallicity-luminosity relation, especially in the young RC. This empirical finding is consistent with the theoretical findings as the variation in the I-band magnitude can be attributed to systematic trends with metallicity (Sarajedini, 1999), suggesting that population effects may be weaker than previously believed. However, the I-band magnitude exhibits little dependence and insignificant correlation with age, consistent with past empirical studies but inconsistent with theoretical studies (Udalski, 2000; Girardi & Salaris, 2001), so population effects cannot be completely disregarded.

Additionally, the multiband approach recommended by Girardi (2016) should not be used for distance estimations in the K-band and I-band. While this method was more accurate for averaging the distance predictions from the K-band and I-band mean magnitude than from the K-band and I-band relations, using solely the mean K-band magnitude would be a more accurate approach.

Apart from the magnitude relations, isochrones should be avoided as a theoretical model when evaluating the RC as a distance indicator. Since isochrones illustrate the changes of a star's property as it evolves, it would exhibit a direct relation between metallicity and age. Contrarily, this study shows metallicity decreases with age in the RC, so fitting an isochrone to RC stars from different clusters, like Grocholski & Sarajedini (2002), cannot properly reflect RC trends. Instead, future studies should use multiple isochrones of different ages and metallicities to reflect the varying properties of stars and the inverse relation between age and metallicity, similar to Girardi (2016), and reveal more accurate trends.

Limitations and Future Directions

This study recognizes several limitations and potential future directions to resolve them.

The crossmatching method based on right ascension and declination is susceptible to many potential errors that hinder the validity of the data. Stars may have slightly changed stellar coordinates between the times of each sky survey, specifically between *Gaia* and *Gaia*-ESO. Unfortunately, this change could not be accounted for because the time between the two surveys could not be found. Moreover, *Gaia*-ESO has a relatively small database size of 114,324 sources (Gilmore, 2022) compared to *Gaia* DR3 with a database size of 1,811,709,771 sources (Vallenari et al., 2022). These issues likely caused cluster data to not completely crossmatch, sources with no crossmatches to be removed, and crossmatched RC data to not accurately represent the actual population's properties. Future studies should use larger databases with source IDs, such as LAMOST, to fully and more accurately crossmatch sources.

As for testing the relations, limiting the testing of the I-band mean magnitude and I-band metallicity-luminosity relation to the old RC likely caused the I-band relation to produce a large error as it was not directly fitted to solely the old RC. Additionally, the extent of population effects of this study's data and trends were not directly quantified with theoretical data. Future studies should reassess and further investigate these potential I-band relations separated by age with more data and with relation to theoretical models.

Conclusion

Red clump stars have increased potential in producing more accurate distance estimations when stratified by age, especially in the K-band and I-band metallicity-luminosity relation. Because of their variation and relations with metallicity, studies cannot solely rely on the mean I-band nor K-band red clump magnitude to estimate distances, but the appropriate distance estimation method would depend on the age and passband. In addition, population effects in the I-band may be weaker than previously believed, and studies using theoretical models should account for the red clump's inverse relation between metallicity and age. These findings will be crucial in discovering new distance methods for red clump stars to calibrate other distance indicators on the distance ladder and estimate distances more accurately.

References

Aidelman, Y., Cidale, L. S., Zorec, J., & Arias, M. L. (2012). Open clusters-I. Fundamental parameters of B stars in NGC 3766 and NGC 4755. *Astronomy & Astrophysics*, *544*, A64. https://doi.org/10.1051/0004-6361/201219069

Alves, D. R. (2000). K-band calibration of the red clump luminosity. *The Astrophysical Journal*, *539*(2), 732. https://doi.org/10.1086/309278

Baume, G., Vázquez, R. A., Carraro, G., & Feinstein, A. (2003). Photometric study of the young open cluster NGC 3293. *Astronomy & Astrophysics*, *402*(2), 549-564. https://doi.org/10.1051/0004-6361:20030223

Bilir, S., Ak, T., Ak, S., Yontan, T., & Bostancı, Z. F. (2013a). A new absolute magnitude calibration for red clump stars. *New Astronomy*, *23*, 88-97. https://doi.org/10.1016/j.newast.2013.03.006

Bilir, S., Önal, Ö., Karaali, S., Cabrera-Lavers, A., & Cakmak, H. (2013b). Luminosity–colour relations for red clump stars. *Astrophysics and Space Science*, *344*, 417-427. https://doi.org/10.1007/s10509-012-1342-9

Bovy, J., Nidever, D. L., Rix, H. W., Girardi, L., Zasowski, G., Chojnowski, S. D., ... & Zamora, O. (2014). The APOGEE red-clump catalog: precise distances, velocities, and high-resolution elemental abundances over a large area of the milky way's disk. *The Astrophysical Journal*, *790*(2), 127. https://doi.org/10.1088/0004-637X/790/2/127

Cannon, R. D. (1970). Red giants in old open clusters. *Monthly Notices of the Royal Astronomical Society*, *150*(1), 111-135. https://doi.org/10.1093/mnras/150.1.111

Cole, A. A., Skillman, E. D., Tolstoy, E., Gallagher III, J. S., Aparicio, A., Dolphin, A. E., ... & Weisz, D. R. (2007). Leo A: a late-blooming survivor of the epoch of reionization in the local group. *The Astrophysical Journal*, *659*(1), L17. https://doi.org/10.1093/mnras/150.1.111

Davidge, T. J. (2005). The evolved stellar content of NGC 147, NGC 185, and NGC 205. *The Astronomical Journal*, *130*(5), 2087. https://doi.org/10.1093/mnras/150.1.111

Gilmore, G. (2022). ESO public survey programme Gaia-ESO spectroscopic survey, Data Release DR5. ESO. https://www.eso.org/rm/api/v1/public/releaseDescriptions/191.

Girardi, L., & Salaris, M. (2001). Population effects on the red giant clump absolute magnitude, and distance determinations to nearby galaxies. *Monthly Notices of the Royal Astronomical Society*, *323*(1), 109-129. https://doi.org/10.1046/j.1365-8711.2001.04084.x

Girardi, L. (2016). Red clump stars. *Annual Review of Astronomy and Astrophysics*, *54*, 95-133. https://doi.org/10.1146/annurev-astro-081915-023354

Grocholski, A. J., & Sarajedini, A. (2002). WIYN open cluster study. X. The K-band magnitude of the red clump as a distance indicator. *The Astronomical Journal*, *123*(3), 1603. https://doi.org/10.1086/339027

Jackson, R. J., Jeffries, R. D., Wright, N. J., Randich, S., Sacco, G., Bragaglia, A., ... & Jiménez-Esteban, F. (2022). The Gaia–ESO Survey: Membership probabilities for stars in 63 open and 7 globular clusters from 3D kinematics. *Monthly Notices of the Royal Astronomical Society*, *509*(2), 1664-1680. https://doi.org/10.1093/mnras/stab3032

Kniazev, A. Y., Grebel, E. K., Pustilnik, S. A., Pramskij, A. G., & Zucker, D. B. (2005). Spectrophotometry of Sextans A and B: chemical abundances of H II regions and planetary nebulae. *The Astronomical Journal*, *130*(4), 1558. https://doi.org/10.1086/432931

Laney, C. D., Joner, M. D., & Pietrzyński, G. (2012). A new Large Magellanic Cloud K-band distance from precision measurements of nearby red clump stars. *Monthly Notices of the Royal Astronomical Society*, *419*(2), 1637-1641. https://doi.org/10.1111/j.1365-2966.2011.19826.x

Lee, M. G., & Kim, S. C. (2000). Stellar populations of the Sagittarius dwarf irregular galaxy. *The Astronomical Journal*, *119*(2), 777. https://doi.org/10.1086/301211

Mallory, K., Calzetti, D., & Lin, Z. (2022). Dust Emission as a Function of Stellar Population Age in the Nearby Galaxy M33. *The Astrophysical Journal*, *933*(2), 156. https://doi.org/10.3847/1538-4357/ac7227

Marrese, P. M., Marinoni, S., Fabrizio, M., & Altavilla, G. (2019). Gaia Data Release 2. Cross-match with external catalogues: algorithms and results. *Astronomy and Astrophysics*, *621*, A144. https://doi.org/10.1051/0004-6361/201834142

Nataf, D. M., Cassisi, S., Casagrande, L., Yuan, W., & Riess, A. G. (2021). On the color–metallicity relation of the red clump and the reddening toward the Magellanic Clouds. *The Astrophysical Journal*, *910*(2), 121. https://doi.org/10.3847/1538-4357/abe530

Paczyński, B., & Stanek, K. Z. (1998). Galactocentric distance with the OGLE and Hipparcos red clump stars. *The Astrophysical Journal*, *494*(2), L219. https://doi.org/10.1086/311181

Parada, J., Heyl, J., Richer, H., Ripoche, P., & Rousseau-Nepton, L. (2021). Carbon stars as standard candles–II. The median J magnitude as a distance indicator. *Monthly Notices of the Royal Astronomical Society*, *501*(1), 933-947. https://doi.org/10.1093/mnras/staa3750

Percival, S. M., & Salaris, M. (2003). An empirical test of the theoretical population corrections to the red clump absolute magnitude. *Monthly Notices of the Royal Astronomical Society*, *343*(2), 539-546. https://doi.org/10.1046/j.1365-8711.2003.06691.x

Perryman, M. A., Lindegren, L., Kovalevsky, J., Hoeg, E., Bastian, U., Bernacca, P. L., ... & Petersen, C. S. (1997). The HIPPARCOS catalogue. *Astronomy and Astrophysics*, *Vol. 323*, p. *L49-L52*, *323*, L49-L52. https://ui.adsabs.harvard.edu/abs/1997A%26A...323L..49P/abstract

Pietrzyński, G., Górski, M., Gieren, W., Laney, D., Udalski, A., & Ciechanowska, A. (2010). The Araucaria project. Population effects on the V-and I-band magnitudes of red clump stars. *The Astronomical Journal*, *140*(4), 1038. https://doi.org/10.1088/0004-6256/140/4/1038

Piotto, G., King, I. R., Djorgovski, S. G., Sosin, C., Zoccali, M., Saviane, I., ... & Renzini, A. (2002). HST color-magnitude diagrams of 74 galactic globular clusters in the HST and bands. *Astronomy & Astrophysics*, *391*(3), 945-965. https://doi.org/10.1051/0004-6361:20020820

Pucha, R., Carlin, J. L., Willman, B., Strader, J., Sand, D. J., Bechtol, K., ... & Romanowsky, A. J. (2019). Hyper Wide Field Imaging of the Local Group Dwarf Irregular Galaxy IC 1613: An Extended Component of Metal-poor Stars. *The Astrophysical Journal*, *880*(2), 104. https://doi.org/10.3847/1538-4357/ab29fb

Reid, I. N. (1999). The HR diagram and the Galactic distance scale after Hipparcos. *Annual Review of Astronomy and Astrophysics*, *37*(1), 191-237. https://doi.org/10.1146/annurev.astro.37.1.191

Rieke, G. H., & Lebofsky, M. J. (1985). The interstellar extinction law from 1 to 13 microns. *The Astrophysical Journal*, *288*, 618-621. https://doi.org/10.1086/162827

Ruiz-Lara, T., Gallart, C., Monelli, M., Fritz, T. K., Battaglia, G., Cassisi, S., ... & Salazar-González, J. J. (2021). Dissecting the stellar content of Leo I: a dwarf irregular caught in transition. *Monthly Notices of the Royal Astronomical Society*, *501*(3), 3962-3980. https://doi.org/10.1093/mnras/staa3871

Sarajedini, A. (1999). WIYN open cluster study. III. The observed variation of the red clump luminosity and color with metallicity and age. *The Astronomical Journal*, *118*(5), 2321. https://doi.org/10.1086/301112

Sohn, S. T., Majewski, S. R., Munoz, R. R., Kunkel, W. E., Johnston, K. V., Ostheimer, J. C., ... & Cooper, M. C. (2007). Exploring halo substructure with giant stars. X. Extended dark matter or tidal disruption?: The case for the Leo I dwarf spheroidal galaxy. *The Astrophysical Journal*, *663*(2), 960. https://doi.org/10.1086/518302

Tully, R. B., Rizzi, L., Dolphin, A. E., Karachentsev, I. D., Karachentseva, V. E., Makarov, D. I., ... & Shaya, E. J. (2006). Associations of dwarf galaxies. *The Astronomical Journal*, *132*(2), 729. https://doi.org/10.1086/505466

Tosi, M., Pulone, L., Marconi, G., & Bragaglia, A. (1998). Old open clusters: the interesting case of Berkeley 21. *Monthly Notices of the Royal Astronomical Society*, *299*(3), 834-844. https://doi.org/10.1046/j.1365-8711.1998.01812.x

Udalski, A. (1998). Optical gravitational lensing experiment. population effects on the mean brightness of the red clump stars. *arXiv preprint astro-ph/9807095*. https://doi.org/10.48550/arXiv.astro-ph/9807095

Udalski, A. (2000). The Optical gravitational lensing experiment: Red clump stars as a distance indicator. *The Astrophysical Journal*, *531*(1), L25. https://doi.org/10.1086/312513

Vallenari, A., Brown, A. G. A., & Prusti, T. (2022). Gaia Data Release 3. Summary of the content and survey properties. *Astronomy & Astrophysics*, *616*. https://doi.org/10.1051/0004-6361/202243940

Venn, K. A., Lennon, D. J., Kaufer, A., McCarthy, J. K., Przybilla, N., Kudritzki, R. P., ... & Smartt, S. J. (2001). First stellar abundances in NGC 6822 from VLT-UVES and Keck-HIRES spectroscopy. The Astrophysical Journal, 547(2), 765. https://doi.org/10.1086/318424

Weisz, D. R., Dalcanton, J. J., Williams, B. F., Gilbert, K. M., Skillman, E. D., Seth, A. C., ... & Zaritsky, D. (2011). The ACS nearby galaxy survey treasury. VIII. The global star formation histories of 60 dwarf galaxies in the local volume. *The Astrophysical Journal*, *739*(1), 5. https://doi.org/10.1088/0004-637X/739/1/5

Supplemental Tables

Supplemental Table 1. K-band cluster red clump data (n=24). For each cluster, after isolating the red clump from *Gaia*, 2MASS, and *Gaia*-ESO data, the mean K-band absolute magnitude $M_{K,\,RC}$, color $(J-K)_{RC}$, and metallicity $[Fe/H]_{RC}$ were calculated. The cluster's distance modulus $(m-M)_0$, reddening E(B-V, and age were obtained from previous studies as indicated by the reference column.

Cluster	RA (°)	Dec (°)	$M_{K,\,RC}$ (mag)	$(J-K)_{RC}$ (mag)	$[Fe/H]_{RC}$ (dex)	N	$(m-M)_0$ (mag)	E(B-V) (mag)	Log Age	Ref
Br32	104.51	6.64	-1.67 ± 0.330	0.60 ± 0.050	-0.31 ± 0.133	32	12.50	0.15	9.72	1
Br81	285.43	-0.45	-1.70 ± 0.735	0.64 ± 0.059	-0.16 ± 0.205	103	12.39	1.00	9.00	2
Loden165	159.06	-58.76	-1.54 ± 0.203	0.57 ± 0.053	-0.32 ± 0.229	3	11.39	0.25	9.48	2
M67	132.90	11.85	-1.37 ± 0.514	0.62 ± 0.027	-0.03 ± 0.048	9	9.80	0.04	9.54	2, 3
NGC104	5.67	-72.07	-1.26 ± 0.218	0.56 ± 0.048	-0.72 ± 0.184	25	13.37	0.04	10.08	2, 4
NGC2141	90.74	10.47	-1.87 ± 0.496	0.57 ± 0.038	-0.16 ± 0.170	87	13.12	0.40	9.26	2
NGC2158	91.87	24.10	-1.83 ± 0.379	0.67 ± 0.049	-0.20 ± 0.131	112	13.49	0.36	9.30	2
NGC2244	97.98	4.91	-1.37 ± 0.068	0.55 ± 0.031	-0.27 ± 0.110	3	11.15	0.48	6.60	2
NGC2264	100.23	9.66	-1.48 ± 0.336	1.06 ± 0.144	-0.18 ± 0.241	36	9.40	0.07	6.60	2
NGC2355	109.27	13.76	-1.49 ± 0.269	0.56 ± 0.040	-0.15 ± 0.188	13	10.92	0.14	8.95	2
NGC2420	114.60	21.60	-1.56 ± 0.261	0.59 ± 0.029	-0.19 ± 0.073	15	11.97	0.05	9.34	2
NGC2516	119.45	-60.90	-1.72 ± 0.322	0.67 ± 0.061	-0.26 ± 0.212	50	8.09	0.11	8.10	2

Cluster	RA (°)	Dec (°)	$M_{K, RC}$ (mag)	$(J-K)_{RC}$ (mag)	$[Fe/H]_{RC}$ (dex)	N	$(m-M)_0$ (mag)	E(B-V) (mag)	Log Age	Ref
NGC2808	138.00	-64.80	-1.36 ± 0.446	0.62 ± 0.023	-1.09 ± 0.162	7	14.91	0.22	10.03	2
NGC3293	158.98	-58.18	-1.45 ± 0.319	0.58 ± 0.070	-0.05 ± 0.113	8	12.20	0.29	6.90	5
NGC3766	174.05	-61.65	-1.44 ± 0.217	0.64 ± 0.056	-0.19 ± 0.173	9	11.61	0.22	7.49	6
NGC4815	194.50	-64.85	-1.80 ± 0.280	0.57 ± 0.062	-0.40 ± 0.250	9	11.99	0.70	8.75	2
NGC5927	232.00	-50.70	-1.62 ± 0.404	0.59 ± 0.049	-0.43 ± 0.072	74	14.43	0.45	10.10	2
NGC6005	238.95	-57.42	-1.53 ± 0.367	0.63 ± 0.040	-0.18 ± 0.299	10	12.16	0.45	9.08	2
NGC6253	254.65	-52.70	-1.62 ± 0.619	0.66 ± 0.059	-0.16 ± 0.208	215	10.90	0.28	9.48	2
NGC6259	255.19	-44.67	-1.81 ± 0.410	0.68 ± 0.102	-0.12 ± 0.175	55	11.61	0.66	8.32	2
NGC6530	271.09	-24.33	-1.75 ± 0.001	0.60 ± 0.035	0.00 ± 0.000	2	10.48	0.35	6.00	2
Trumpler14	161.10	-59.73	-1.61 ± 0.320	0.51 ± 0.015	-0.06 ± 0.075	4	12.30	0.65	6.30	2
Trumpler20	189.90	-60.63	-1.44 ± 0.235	0.59 ± 0.063	-0.14 ± 0.182	17	12.39	0.35	9.15	2
Trumpler5	99.10	9.45	-1.61 ± 0.290	0.59 ± 0.050	-0.36 ± 0.177	53	11.90	0.60	9.70	2

1) Tosi et al. (2007), 2) Jackson et al. (2021), 3) Grocholski & Sarajedini (2002), 4) Piotto et al. (2002), 5) Baume et al. (2003), 6) Aidelman et al. (2012)

Supplementary Table 2. I-band cluster red clump data from Pietrzyński et al. (2010) and other studies (n=13). For each cluster's red clump, the I-band absolute magnitude $M_{I, RC}$, color $(V-I)_{RC}$, metallicity $[Fe/H]_{RC}$, and reddening E(B-V) were obtained and calculated from Pietrzyński et al. (2010), and the age is obtained from other previous studies as indicated by the reference column.

Cluster	$M_{I, RC}$ (mag)	$(V-I)_{RC}$ (mag)	$[Fe/H]_{RC}$ (dex)	$(m-M)_0$ (mag)	E(B-V) (mag)	Log Age	Ref
NGC 6822	-0.37 ± 0.004	1.06 ± 0.006	-1.06 ± 0.03	23.49	0.23	9.48	1, 2
IC 1613	-0.46 ± 0.007	0.83 ± 0.009	-1.50 ± 0.02	24.34	0.03	10.00	3, 4
DDO 74	-0.74 ± 0.010	0.84 ± 0.012	-1.70 ± 0.06	22.05	0.04	9.74	5, 6
NGC 185	-0.09 ± 0.003	0.81 ± 0.005	-1.16 ± 0.03	23.95	0.18	9.00	7

Cluster	$M_{I,RC}$ (mag)	$(V-I)_{RC}$ (mag)	$[Fe/H]_{RC}$ (dex)	$(m-M)_0$ (mag)	E(B-V) (mag)	Log Age	Ref
NGC 147	-0.05 ± 0.003	0.77 ± 0.004	-1.21 ± 0.03	24.15	0.17	9.50	7
DDO 69	-0.53 ± 0.015	0.89 ± 0.017	-2.02 ± 0.08	24.50	0.02	9.90	8
DDO 75	-0.72 ± 0.008	0.72 ± 0.014	-2.15 ± 0.04	25.60	0.04	9.20	9
M33	-0.31 ± 0.003	0.95 ± 0.004	-0.97 ± 0.03	24.65	0.05	6.48	10
E594-004	-1.29 ± 0.013	1.05 ± 0.021	-2.37 ± 0.06	25.54	0.12	8.48	11
Antlia	-0.63 ± 0.007	0.70 ± 0.012	-1.92 ± 0.01	25.89	0.08	10.00	12
E410-005	-0.50 ± 0.007	0.82 ± 0.009	-1.81 ± 0.02	26.42	0.01	10.08	13
UGC 9128	-0.73 ± 0.009	0.80 ± 0.013	-2.08 ± 0.03	26.72	0.02	9.00	14
E294-010	-0.29 ± 0.013	0.79 ± 0.016	-1.6 ± 0.02	26.39	0.01	10.00	15

1) Venn et al. (2000), 2) Zhang et al. (2021), 3) Pucha et al. (2019), 4) Parada et al. (2020), 5) Sohn et al. (2007), 6) Ruiz-Lara et al. (2020), 7) Davidge (2005), 8) Cole et al. (2007), 9) Kniazev et al. (2005), 10) Mallory et al. (2022), 11) Lee & Kim (1999), 12) Piersimoni et al. (1999), 13) Benítez-Llambay et al. (2015), 14) Tully et al. (2006), 15) Weisz et al. (2011)

Supplementary Table 3: Results of the K-band and I-band regression analysis. After conducting OLS analysis on the K-band and I-band red clump data stratified by age at 2 Gyr, the K-band and I-band regression coefficients represented by ax+b, where a is the coefficient and b is the constant term, and their standard deviations, R^2-coefficients, and root mean square error (RMS) were calculated.

Relation	a	b	R^2-coefficient	RMS
All M_K vs. color	-1.2452 ± 0.812	-0.8338 ± 0.491	0.101	0.158
Young M_K vs. color	-0.8684 ± 0.981	-1.0940 ± 0.590	0.058	0.134
Old M_K vs. color	-1.2298 ± 1.868	-0.7757 ± 1.121	0.067	0.156
All M_K vs. metallicity	-0.2424 ± 0.143	-1.6421 ± 0.049	0.116	0.153
Young M_K vs. metallicity	0.0992 ± 0.474	-1.5892 ± 0.091	0.244	0.120
Old M_K vs. metallicity	-0.2254 ± 0.150	-1.6033 ± 0.075	0.004	0.159
All M_K vs. age	0.0043 ± 0.028	-1.6175 ± 0.241	0.001	0.163
Young M_K vs. age	-0.0382 ± 0.038	-1.3039 ± 0.305	0.139	0.128
Old M_K vs. age	0.1893 ± 0.178	-3.3526 ± 1.730	0.077	0.153

Relation	a	b	R^2-coefficient	RMS
All M_I vs. color	-0.7609 ± 0.839	0.1301 ± 0.718	0.070	0.300
Young M_I vs. color	-1.4821 ± 1.812	0.6563 ± 1.585	0.182	0.372
Old M_I vs. color	0.0634 ± 0.814	-0.4982 ± 0.686	0.001	0.198
All M_I vs. metallicity	0.5916 ± 0.122	0.4649 ± 0,209	0.681	0.176
Young M_I vs. metallicity	0.6496 ± 0.185	0.5056 ± 0.340	0.804	0.182
Old M_I vs. metallicity	0.4174 ± 0.194	0.2238 ± 0.317	0.435	0.149
All M_I vs. age	9.275×10-5 ± 2.21×10-5	-0.5625 ± 0.145	0.016	0.315
Young M_I vs. age	-0.0942 ± 0.229	0.1660 ± 1.949	0.053	0.400
Old M_I vs. age	-0.3989 ± 0.326	3.4787 ± 3.208	0.200	0.178

Supplementary Table 4. K-band and I-band testing data from Percival & Salaris (2003) (n=6). To test the distance estimation methods in the I-band, K-band, and the multiband approach, K-band and I-band data of the old RC was collected from Percival & Salaris (2003) to calculate and compare the RMS of each method.

Cluster	$M_{K,RC}$ (mag)	$M_{I,RC}$ (mag)	$[Fe/H]_{RC}$ (dex)	$(m-M)_0$ (mag)	E(B-V) (mag)	Log Age
Be 39	-1.434 ± 0.094	-0.107 ± 0.100	-0.15 ± 0.09	12.97	0.11	8.88
M67	-1.614 ± 0.097	-0.203 ± 0.103	0.02 ± 0.06	9.60	0.04	8.6
Mel 66		-0.197 ± 0.084	-0.38 ± 0.06	13.22	0.14	8.65
NGC 188		-0.091 ± 0.092	-0.03 ± 0.06	11.17	0.09	8.78
NGC 2420	-1.676 ± 0.099		-0.44 ± 0.06	11.94	0.05	8.3
47 Tuc	-1.280 ± 0.072	-0.149 ± 0.081	-0.7 ± 0.10	13.25	0.04	9.04